High-Shear Granulation Modeling Using a Discrete Element Simulation Approach

Justin A. Gantt and Edward P. Gatzke

Department of Chemical Engineering
The University of South Carolina
301 Main Street, Columbia , SC 29201

Abstract

This work develops a method for prediction of dynamic changes in particle size distributions (PSD) of high-shear granulation systems using a discrete element simulation technique. This method allows for direct evaluation of particle interactions based on multi-dimensional descriptions of particle parameters. Pouw et al. [37] proposed the use of a volume-based Population Balance Equation (PBE) model with the volume of solid, liquid, and gas in each particle as internal parameters to predict result of particle interactions. This paper extends on the work of Pouw et al. by using a discrete element simulation approach rather than direct application of population balance equations to determine the evolution of particle size distributions. This is accomplished by simulating the effects of particle interactions based on physically significant coalescence criteria.

Three granule modification mechanisms are used in the proposed method: coalescence, consolidation, and breakage. Two types of coalescence are modeled in this simulation. In Type I coalescence, granules are stopped solely by viscous dissipation of the binder layer before the granule solid surfaces touch, whereas Type II coalescence occurs when weak deformable granules come into contact with their solid surfaces and the granule surfaces then bind together. Consolidation, the escape of air from granules due to compaction following collisions, is described by an exponential relationship related to the porosity of each individual simulated particle. One may assume that breakage will occur when there is sufficient externally applied kinetic energy to deform and shear a granule. Breakage can be determined based on whether the Stokes deformation number for a particle exceeds a critical value.

One objective of this work is to move toward modeling and simulation methods that allow for dynamic changes in operating conditions at any time in a batch run. Current empirically based coalescence kernels used in population balance based models are generally developed using static operating conditions, limiting the model validity for online control applications. The main contribution of this work lies in the observation that when using this type of simulation model, the physics of the granulation system can be altered more easily than modeling the granulation process using traditional population balance. Systems exhibiting a wide range of deformations can be modeled to determine boundaries for Type I coalescence, Type II coalescence, or rebound events based on physical arguments rather than extrapolation of empirically based coalescence kernels. Using similar initial and operating conditions, the discrete element simulation is shown to produce results similar to population balance results. To examine the extended flexibility of the new modeling method, several open-loop simulations using this method are presented in this paper to display how a process would dynamically react to changes in operating conditions.

1 Introduction

Granulation is a size enlargement technique where small, dry particles agglomerate to form larger aggregate particles by means of binder addition and process agitation. Types of granulation processes include fluidized bed, pan, drum, and high-shear mixer granulation. Size enlargement is used in industry for many purposes: elimination of dust to mitigate handling hazards or minimize losses, increased bulk density during storage, control of product solubility, control of porosity, improved product appearance, improved heat transfer characteristics, etc. [10]. For most size enlargement processes, the granule size distribution is a property of primary importance, directly related to product quality. Modeling and control of the evolution of granule size distributions can be investigated using a variety of modeling techniques.

Models based on Population Balance Equations (PBE's) are crucial in the field of particulate process analysis because these models allow for the calculation of size distribution, as well as the determination of controlling granulation mechanisms. PBEs are particularly useful with respect to process control through the use of sensitiv-

ity analysis to determine how changes to input conditions effect product quality [10]. In most cases, the analytical solution to a population balance is not trivial. Many methods for the modeling of aggregate processes using discrete population balances have been proposed, where particles of different sizes exist in discrete groups that interact collectively with particles in other groups. Various researchers (Batterham et al., 1981[5], Ramkrishna et al., 1985[38], Hounslow et al., 1988[14]), pioneered the use of numerical techniques to solve a PBE in order to find a discretized solution for these agglomerate processes.

Modeling of a granulation process using only a one-dimensional PBE, as is commonly done in practice, will not suffice in most situations because it will not capture the true intergranular behavior between particles [17, 4]. Several independent granule properties such as porosity, pore saturation, and moisture fraction have been proven to strongly effect granular behavior [20, 16]. These properties have been found to be most easily modeled when the intrinsic particle parameter used in the PBE is the particle volume [37]. Using volume as the intrinsic parameter in a population balance allows for the PBE to be consistent with the mass balance; this is not necessarily true when particle size is used as an intrinsic parameter because changes in particle diameter are not additive. Pouw et al. [37] proposed a multi-dimensional population balance, which uses volume as the intrinsic parameter. This volume-based model tracks the evolution of the volume of solids, volume of liquid, and volume of air of a nucleated granule at each time step. Other models have been established using these intrinsic parameters to calculate granulate parameters such as pore saturation, porosity, and liquid fraction. Kumar and Ramkrishna [28] have shown that most discretized population balance equations for agglomerate processes often over-predict number densities for large particles, so other methods for predicting particle size distributions would be beneficial for properly estimating aggregate-breakage process parameters [28, 29].

This work extends current granulation models that use volume as the intrinsic parameter by use of a dynamic simulation approach, with some characteristics of Monte Carlo modeling. The proposed discrete element method allows for the determination of particle size distributions as well as pore saturation, porosity, or other properties of granules in each size class. In this simulation work, a finite number of particle are initially given velocity and position values in a three dimensional space. These particles are also initialized with internal solid, liquid, and gas volume values. Using these internal parameters, granular properties such as porosity, pore saturation, liquid content [47, 46], moisture fraction, size class, liquid binder thickness [31], granule yield stress [44], and strain are calculated based on models for intragranular properties. Multiple simulations are performed and averaged to mitigate effects of random initial conditions and limited sampling size.

Granulation rates are controlled by several key particle changing mechanisms: coalescence, breakage, consolidation, attrition, and evaporation [19, 31, 32]. Some mechanisms such as breakage and coalescence apply to the entire particle, while others only apply to only a certain phase (i.e. consolidation only applies to air volume and evaporation only applies to liquid volume). To simplify the simulation process, only three primary mechanisms are taken into account in this work: coalescence, consolidation, and breakage.

Coalescence between particles is based on a physically significant coalescence kernel that depends on the following dimensionless parameters: (1) the viscous Stokes number St_v, a measure of the kinetic energy of a particle made dimensionless with respect to the scale of viscous dissipation of the liquid binder layer, (2) the Stokes deformation number St_{def} , which is the ratio of the impact kinetic energy to the plastic deformation of the particle, (3) the ratio of the plastic yield stress to the elastic modulus, Y_d/E^*, and (4) the ratio of the liquid layer thickness to the height of the surface asperities, h_o/h_a. Each of these dimensionless parameters are calculated and continuously updated during the simulation based on the varying intrinsic parameters of each individual particle.

Using this dynamic simulation method, several tests have been performed to simulate granular behavior under different operating conditions. The dynamic results of the simulation show an induction period where the liquid in the particle becomes compressed through the pores due to consolidation until the liquid layer thickness of each particle reaches a level capable of supporting successful collisions resulting in coalescence. Rapid particle growth is observed following this induction period. When five size classes are used to describe the granulation process, the results found using this approach are analogous to results found by Pouw et al. using an extended population balance model [37]. Dynamic effects observed using analytical methods can also be observed using the discrete element simulation approach. These effects include increasing pore saturation and a decreasing porosity due to consolidation,

2 Theory

The proposed simulation method is developed from a collection of physics-based models. The discrete element simulation method uses fundamental expressions for determination of coalescence or rebound when individual particle collisions occur. The details of these expressions are described in the following sections.

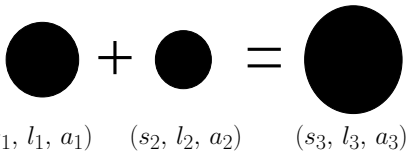

Figure 1: Coalescence of two particles using volume as the internal property.

2.1 Basic particle representation

It is assumed that the granules in the simulation are in a nucleated particle matrix each with an identical initial pore saturation due to an assumed uniform binder dispersion in the granulator. The binder is assumed to be a compressible Newtonian fluid and the granule is assumed to react as a simple elastic-plastic solid as described by Liu et al. [32]. Due to an assumed uniform binder dispersal method, the granules are assumed to follow a normal initial nuclei distribution. Using granule volume as the intrinsic parameter in the simulation, Pouw et al. [37] proposed a method where a particle volume can be described as a vector $\underline{G}$ composed of the granule solid volume s, liquid binder volume l, and air volume a:

$$\underline{G} = [s \quad l \quad a]^T \tag{1}$$

where the total volume of granule i is the sum of the three components:

$$V_i = s_i + l_i + a_i \tag{2}$$

Using this initial composition of phases in each granule, internal granule properties such as porosity ε, moisture fraction w, pore saturation S, and liquid fraction L, can be calculated as:

$$\begin{array}{rcl} \varepsilon_i & = & \frac{l_i+a_i}{s_i+l_i+a_i} \\ w_i & = & \frac{l_i}{s_i} \\ S_i & = & \frac{l_i}{l_i+a_i} \\ L_i & = & \frac{l_i}{s_i+l_i+a_i} \end{array} \tag{3}$$

Assuming that the densities of each phase are assumed constant, the mass of the granule m, can easily be calculated as well;

$$m_i = \rho_s \cdot s_i + \rho_l \cdot l_i + \rho_a \cdot a_i \tag{4}$$

where ρ_s, ρ_l, and ρ_a are the densities of the solid powder, liquid binder and air, respectively. In the event of coalescence, the volumes and masses of each phase of the coalescing particles are added to calculate the volume and mass of the new particle, while internal parameters such as porosity and moisture fraction are not additive and must be recalculated, see Figure 1.

Pore saturation is a critical parameter for modeling coalescence of granules, as pore saturation can be assumed to be the determining parameter in the calculation of a liquid binder layer on a granule [31]. If the pore saturation, S, is greater than a critical value, S^*, then the particle is considered oversaturated and the binder layer first appears. Assuming that the binder layer, h_0, is much smaller than the granule diameter, $(h_0 \ll D)$, Liu and Litster [31] derived the binder layer thickness as :

$$h_0 = \begin{cases} \frac{D(L-\varepsilon S^*)}{6}; & L > \varepsilon S^* \\ 0; & L < \varepsilon S^* \end{cases} \tag{5}$$

2.2 Coalescence of surface wet granules

Liu [31] presents a criteria for coalescence among deformable surface-wet granules. This criteria was first derived using contact mechanics described by Johnson [21]. Their model assumes that deformation begins when granules are in physical contact, liquid capillary forces are negligible, the interparticle attractive forces are negligible, and fluid cavitation does not occur during rebound. Their model also neglected breakage following deformation, which will be discussed later. The work presented here considers the collision between two particles with a liquid binder layer present. The collision velocity used is twice the relative velocity of the particles, $2u_0$, where the relative velocity between particles i and j is:

$$u_0 = \frac{\sqrt{\left(v_{x_i} - v_{x_j}\right)^2 + \left(v_{y_i} - v_{y_j}\right)^2 + \left(v_{z_i} - v_{z_j}\right)^2}}{2} \tag{6}$$

Figure 2 shows the stages of a granule collision. At the initial approach stage, only the binder layers of the two granules touch; the particles i and j are at a distance of $h_{0i} + h_{0j}$ from each other. Deformation of the liquid layers will dissipate some of the kinetic energy caused by the collision. If all the kinetic energy of the crash is dissipated by the binder layer, then the collision velocities of the granules following viscous dissipation of energy, u_1, equals zero and the particles coalesce at the binder layer through Type I coalescence. If the kinetic energy is not dissipated, then the solid surfaces of the particles will first come into contact when the surface asperities touch at a distance of $2h_a$. The relative velocity of the crash has now slowed to $2u_1$ due to the binder layer and the surface asperities. The granules then touch and deform some area, A. Rebound begins as the stored elastic energy is released at a relative velocity of $2u_2$. Once again, the binder layer will dissipate the energy caused by the rebound. If the binder layer is able to dissipate the remaining kinetic energy, the granules will stick due to Type II coalescence. If the energy is not dissipated, the granules will completely rebound at a relative velocity of $2u_3$. Details and complete explanation of these parameters is provided in [31].

The collision velocity of granules when the surface asperities touch, u_1, is derived by integrating the equation

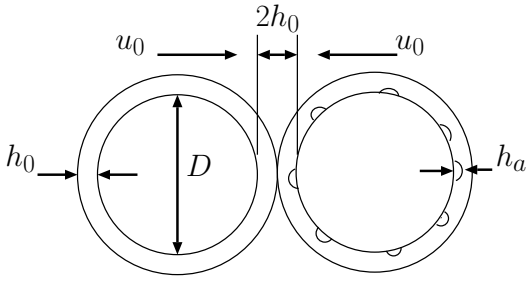

1. Initial approach stage; Type I coalescence may occur.

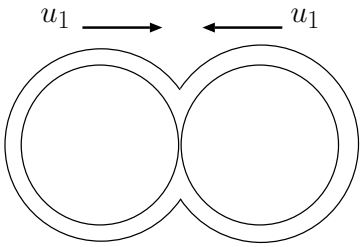

2. Deformation stage; solid layers touch.

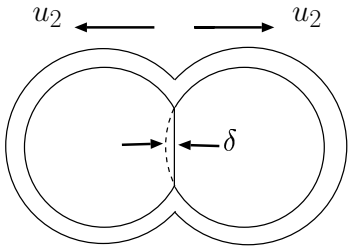

3. Initial separation stage; rebound begins.

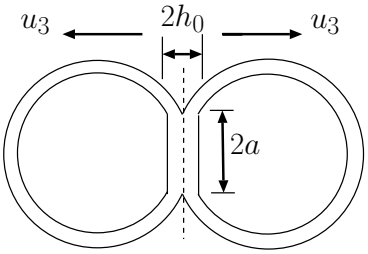

4. Final separation stage; Type II coalscence or rebound occurs.

Figure 2: Current model used to predict coalescence between granules. [31, 19]

of motion. The collision velocity is found to be:

$$u_1 = u_0 \left[1 - \frac{1}{St_v} \ln \left(\frac{h_0}{h_a} \right) \right] \tag{7}$$

where h_0/h_a is the ratio of the binder layer thickness to the height of the surface asperities and St_v is the viscous Stokes number given as [19, 8, 31]:

$$St_v = \frac{8\widetilde{m}u_0}{3\pi\mu\widetilde{D}^2} \tag{8}$$

where $\widetilde{m}$ is the mean harmonic mass, μ is the binder viscosity, and $\widetilde{D}$ is the mean harmonic diameter of particles i and j given by:

$$\widetilde{m} = \frac{m_i m_j}{m_i + m_j} \tag{9}$$

$$\widetilde{D} = \frac{D_i D_j}{D_i + D_j} \tag{10}$$

As previously stated, if the viscous dissipation of the binder layer is sufficient to bring the granule velocity at the binder layer, u_1, equal to or less than zero, then Type I coalescence takes place. The criteria defined by Liu [31] states:

$$St_v < \ln \left(\frac{h_0}{h_a} \right) \tag{11}$$

When the dissipation is not great enough to halt the granules and deformation occurs, the maximum deformed area was derived in Equation 10 of [31] to be:

$$A^* = \pi\widetilde{D}\delta^* = 2u_1 \sqrt{\left[\frac{\pi\widetilde{m}\widetilde{D}}{3Y_d} \right]} \tag{12}$$

where $\delta^*$is the maximum compression distance and Y_d is the yield strength of the granule. Liu [31] used an approximation experimentally developed by Johnson [21], which showed that the yield strength could be approximated as one third of the mean contact pressure. Bull [6] provided a relationship between mean contact pressure, P, and maximum tensile stress, σ_t, by defining each in terms of the maximum contact pressure between two elastic-plastic spherical bodies, P_0:

$$P_0 = \frac{1}{\pi} \left[\frac{24P\left(E^*\right)^2}{\widetilde{D}^2} \right]^{1/3} \tag{13}$$

where P is the contact force between the particles and E^* is the effective Young's modulus between two particles:

$$E^* = \frac{1 - \nu_1^2}{E_1} + \frac{1 - \nu_2^2}{E_2} \tag{14}$$

Here E_1 and E_2 are the Young's modulus of the two granules, and ν_1 and ν_2 are the Poisson ratios. The mean contact pressure, P, was defined by Bull as $\frac{2}{3}P_0$. Furthermore, the maximum tensile stress is defined as a function of the maximum contact pressure by:

$$\sigma_t = \frac{1}{3}(1-2\nu)P_0 \tag{15}$$

Iveson et al. [18] used a model previously derived by Rumpf [40], which assumed that for granules in the funicular or capillary states, the maximum tensile stress could be modeled in terms of internal granular properties by

$$\sigma_t = \frac{1-\varepsilon}{\varepsilon}\frac{SC\,\gamma_l}{D_p}\cos(\theta) \tag{16}$$

where C is a shape factor (6 for spheres), D_p is the diameter of the particles making up the granules, γ_l is the liquid surface tension, and θ is the solid-liquid contact angle (assumed to be zero throughout these simulations).

Combining Equations 15 and 16 and expressing the result in terms of the yield stress results in an expression for the yield stress in terms of internal parameters:

$$Y_d = \frac{2}{3}\frac{\sigma_t}{1-2\nu} = \frac{2}{3-6\nu}\frac{1-\varepsilon}{\varepsilon}\frac{SC\,\gamma_l}{D_p}\cos(\theta) \tag{17}$$

For many solids $\nu = 0.3$ [30, 6], producing a yield stress of $Y_d = \frac{5}{3}\sigma_t$.

The initial rebound velocity as defined by Liu [31] is:

$$u_2 \approx 2.46\sqrt{\frac{Y_d}{E^*}}\left(\frac{\widetilde{m}u_0^2}{2\widetilde{D}^3 Y_d}\right)^{-1/8}\left(1-\frac{1}{St_v}\ln\frac{h_0}{h_a}\right)^{3/4} \tag{18}$$

The permanent deformation, $\delta^{''}$, is defined as the maximum deformation, δ^* minus the extent of elastic recovery, $\delta^{'}$:

$$\delta^{''} = \frac{A^*}{\pi\widetilde{D}} - \sqrt{A^*\pi}\frac{9Y_d}{4E^*} \tag{19}$$

The granule velocity, u_3, at the separation distance when the bridge will rupture, $2h_0$, is defined by Liu as

$$u_3 = u_2 - \frac{3\pi\widetilde{D}^2\left(\delta^{''}\right)^2}{16\widetilde{m}h_0^2}\times$$

$$\left[\left(\frac{h_0^2}{h_a^2}-1\right)+\frac{2h_0}{\delta^{''}}\left(\frac{h_0}{h_a}-1\right)+\frac{2h_0^2}{\left(\delta^{''}\right)^2}\ln\left(\frac{h_0}{h_a}\right)\right] \tag{20}$$

By setting the rebound velocity, $u_3 < 0$, the criteria for Type II coalescence was developed by Liu [31] for the situation in which $\delta^{''} > 0$:

$$\sqrt{\frac{Y_d}{E^*}}St_{def}^{(-9/8)} < \frac{0.172}{St_v}\left(\frac{\widetilde{D}}{h_0}\right)^2\left[1-\frac{1}{St_v}\ln\frac{h_0}{h_a}\right]^{5/4}\times$$

$$\left[\left(\frac{h_0^2}{h_a^2}-1\right)+\frac{2h_0}{\delta^{''}}\left(\frac{h_0}{h_a}-1\right)+\frac{2h_0^2}{\left(\delta^{''}\right)^2}\ln\left(\frac{h_0}{h_a}\right)\right]\times$$

$$\left\{1-7.36\frac{Y_d}{E^*}St_{def}^{-1/4}\left[1-\frac{1}{St_v}\ln\frac{h_0}{h_a}\right]^{-1/2}\right\}^2 \tag{21}$$

where St_{def} is the Stokes deformation number, a measure of the impact kinetic energy of a granule to the plastic deformation of the granule.

$$St_{def} = \frac{\widetilde{m}u_0^2}{2\widetilde{D}^3 Y_d} \tag{22}$$

If there is no permanent deformation present $\left(\delta^{''}\approx 0\right)$, the Type II coalescence criteria was derived by Liu to be:

$$St_v < 2\ln\left(\frac{h_0}{h_a}\right) \tag{23}$$

These conditions can be used to test individual events in the discrete element simulation.

2.3 Coalescence of surface dry granules

During the period of induction, air is being forced out of the granule due to collisions with particles, walls, or the impeller. While the pore saturation remains below the critical level, there is no binder layer present. Despite the lack of a binder layer, it is still possible for granules to coalesce if sufficient binder becomes present in the bond zone following a deformable collision [31]. This is only possible if the granules are highly deformable (high St_{def}) and are near the critical pore saturation. The act of deformation of a granule will force some amount of binder to the bond zone, but new coalescence criteria has to be developed to predict this mechanism. Liu [31] derived coalescence criteria for surface dry particles based on Type II coalescence criteria for surface wet particles. In modeling the coalescence of these dry particles, there is no approach stage ($u_1 = u_0$) and binder is assumed to be present only at the site of the collision. The binder layer thickness, h_0, for the collision was assumed to be the thickness of the permanent deformation, $\delta^{''}$. The permanent deformation for collisions of particles without a binder layer given in [31] is:

$$\delta^{''} = \left(\frac{8}{3\pi}\right)^{1/2}\sqrt{St_{def}}\,\widetilde{D}\left[1-7.36\left(\frac{Y_d}{E^*}\right)St_{def}^{-1/4}\right] \tag{24}$$

Liu and Litster [31] derived the coalescence criteria for surface dry granules to be:

$$\sqrt{\frac{Y_d}{E^*}}St_{def}^{(-9/8)} < \frac{0.172}{St_v}\left(\frac{\widetilde{D}}{h_0}\right)^2\times$$

$$\left[\left(\frac{\delta''}{h_a}\right)^2 - 1\right]\left(1 - 7.36\left(\frac{Y_d}{E^*}\right)St_{def}^{-1/4}\right) \quad (25)$$

2.4 Consolidation

As granules collide against each other or against walls or impellers in granulators, air is slowly forced out of the granule. Consolidation is a very important rate mechanism in granulation, as it controls not only the amount of air inside a particle but also controls the rate that binder is eventually forced out of pores, therefore controlling binder layer height. Several models for consolidation have been described by some form of an exponential decay relationship for porosity as a function of time [16, 37]:

$$\frac{d\varepsilon}{dt} = -k_c\left(\varepsilon - \varepsilon_{min}\right) \quad (26)$$

where ε_{min} is the minimum porosity attainable and k_c is a consolidation rate constant. Substituting the definition of porosity $\varepsilon = (l+a)/(s+l+a)$ and defining $\varepsilon_{min} = l/(s+l)$ results in the following expression for consolidation [46, 37]:

$$\frac{da}{dt} = -k_c\left(\frac{(l+a)(s+l+a)}{s} - \varepsilon_{min}\frac{(s+l+a)^2}{s}\right) \quad (27)$$

Clearly consolidation only affects the air volume of a granule. This model for consolidation was used by Pouw et al. [37] to derive an analytical solution for a population balance.

2.5 Breakage

Breakage occurs in a granulator when the shearing forces are greater than a critical level beyond which a granule cannot remain intact. This means larger particles as well as particles in greater velocity fields have a much greater chance of shearing. Breakage can often greatly effect the final particle size distribution, especially in high-shear granulators. Determining the extent of a role that breakage plays on determining the final PSD can be difficult because the mean granule size may decrease with respect to increased agitator speed for other reasons than pure breakage.

At the present time, only limited theory is available for predicting breakage of wet granules. A quantitative theory was proposed by Tardos et al. [45], where it was concluded that granules will break in a shear field if there is an external kinetic energy surpassing some critical value. This was presented in the form of the Stokes deformation number criteria as:

$$St_{def} > St_{def}^* \quad (28)$$

where St_{def} is altered by introducing a new stress factor that is more general than the dynamic yield strength:

$$St_{def} = \frac{\widetilde{m}u_0^2}{2\widetilde{D}^3\tau(\gamma)} \quad (29)$$

where $\tau(\gamma)$ is the new yield stress described by the Hershel-Buckley model:

$$\tau(\gamma) = Y_d + \mu\,\gamma^{\,n} \quad (30)$$

In this equation, Y_d is the dynamic yield strength, μ is the apparent viscosity, γ is the strain rate, and n is the flow index, and . Tardos et al. [45] make a first assumption that the apparent viscosity is much less than the dynamic yield strength. If $\mu \ll Y_d$, then $\tau(\gamma) \simeq Y_d$ and Equation 29 takes the form of the previous Stokes deformation number, Equation 22.

Another model for breakage of granules was developed by Kenningley et al. [25] for the situation of high-shear granulation. The aforementioned model equated the impact kinetic energy to the energy absorbed by plastic deformation of the granules. The granule strain, ε_m, was calculated using the Kozeny-Carmen equation.

$$\varepsilon_m = \sqrt{\frac{1}{540}\frac{\varepsilon^3}{(1-\varepsilon)^2}\frac{\rho u d_{32}}{\mu}} \quad (31)$$

where d_{32} is the Sauter mean constituent particle size. Again breakage is assumed using this model if the individual strain of a granule exceeds a critical value, $\varepsilon_m > \varepsilon_m^*$.

3 Dynamic simulation

3.1 Current modeling methods: The coalescence kernel

Population balances are the most common method of determining the evolution of particle size distribution for granulation processes. Population balance equation models determine the result of particle-particle interactions based on coalescence kernels. Coalescence kernels are often composed of two parts, a size independent kernel, β_0, and a size dependent kernel, $\beta^*(u,v)$ as seen in Equation 32.

$$\beta(u,v) = \beta_0\beta^*(u,v) \quad (32)$$

Some of the original coalescence kernels proposed by Sastry et al. and Kapur and Fuerstenau [23, 22, 24, 41] are based on purely empirical models. Other coalescence kernels are based on models that rely on probabilities of coalescence [27]. Physically based coalescence kernels are currently being investigated in ongoing research [3, 7, 43, 17, 32]. These models use limiting parameters that are typically derived from a critical value based on

Stokes law. Adetayo and Ennis [2] found a critical granule size based on the conditions for Type I coalescence. Using this critical size, they developed a cut-off kernel. Liu and Litster [32] solved the population balance equation, deriving a kernel by classifying particle-particle interactions as either Type I coalescence or Type II coalescence without permanent deformation, Type II coalescence with permanent deformation, or rebound.

Models based on physical granule and binder properties are more fundamentally sound than their empirical counterparts. Despite this, there is still little information available on the application of physically based coalescence kernels in literature. This can be attributed to several reasons. Adetayo and Ennis [1] attribute this to a lack of knowledge of the granule collision velocity distribution in a granulator. Also, the solution to a population balance equation is not trivial [10, 11]. Analytical solutions are rarely available. When complex coalescence kernels as well as breakage and compaction are present, a PBE solution may only be available numerically. Often with the numerical solution, the computation time may be too unrealistic to be applied to control or optimization of a granulation process. With this in mind, dynamic simulation using a population of individual particles is now considered.

3.2 The simulation process

The proposed dynamic simulation is similar to a Molecular Dynamic Simulation (MDS) [12, 33, 34] in which a molecule is given a position in time and a velocity, and intermolecular forces are calculated by solving Newton's equation of motion. The proposed dynamic simulation technique is used to predict the evolution of a particle size distribution for a group of particles existing in a small volume of a theoretical granulator. The computation proceeds with each granule moving in small increments at each time step with a step representing one second. Collisions are detected and conditions for coalescence, rebound, and breakage are calculated. A dynamic simulation including the known physics of granulation would be beneficial in modeling a granulation process because the simulation allows for easy application of phenomenologically based physical changes to the process. For example, the velocity of the flow field could be altered, the initial binder content in the granule could increase, or a change in the granule yield stress could occur. In each of these examples, the dynamic simulation will determine the evolution of the PSD. Such changes to the PBE may be difficult and time consuming to develop. Figure 3 shows the basis of this simulation technique. Changes in each granule are tracked to predict the evolution of the PSD.

Each particle is initially given a random position in a small three dimensional space to simulate a coalescence

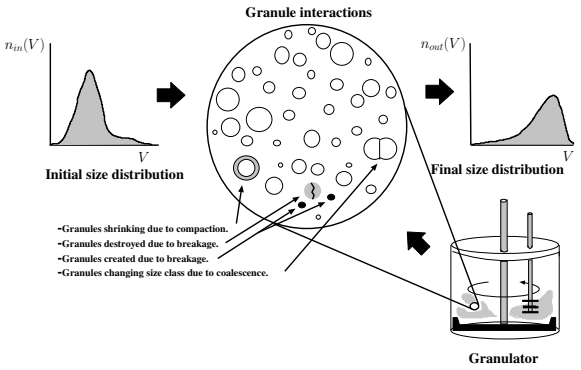

Figure 3: The evolution of the PSD by tracking physical intergranule changes and interactions.

regime of a granulator. Each side measures $2 \times 10^{-3}\, m$ in this work. Initial particle positions are developed such that no two particles initially overlap. Repeating spatial boundary conditions are used for particles that move beyond the borders of the simulation. The granules are each assumed to be spherical, even after coalescence. An initial size distribution of granules is applied to create an initial set of particles to be simulated. The initial size and velocity conditions for the population of particles is arbitrary and can be readily modified for a given experimental system. In this work, each particle has a mean volume of $3 \times 10^{-12}\, m^3$ with a standard deviation of $1 \times 10^{-12}\, m^3$. The particles are then given a randomly determined velocity in each direction in three dimensional space. A normal distribution is used for each velocity component with a mean velocity of 3 m/s and a standard deviation of 1 m/s. The mean velocity of the normal distribution is based on the impeller speed of the granulator by Equation 33:

$$v_{x_i} = \frac{\omega D_g}{2} \tag{33}$$

where v_{x_i} is the velocity of the i^{th} granule in the x direction, ω is the angular velocity of the impeller $(1/s)$ and D_g is the diameter of the granulator, (m). The velocity distribution in each direction will be based on the geometry of the granulator being modeled. For instance, in high-shear granulators, the granules in the radial direction should be far greater than the velocities in the other two directions while in low shear pan or drum granulators, the velocities in each direction are much closer to the same values. For a high-shear granulator modeled in this paper, several distributions will be investigated.

With a known position, velocity in each direction, and particle size, each granule is then given an identical composition of solid, binder, and air. This assumes a perfect distribution of binder between granules. With volumes of solid, liquid, and gas known, the total granule volume V and diameter D is calculated. From Equation 3, the poros-

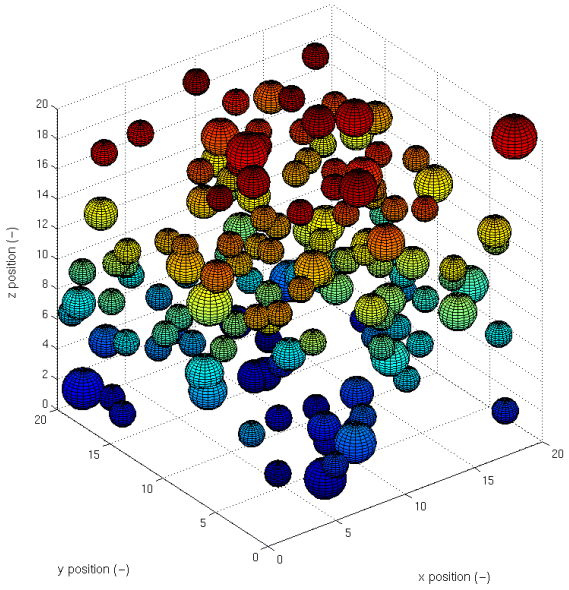

Figure 4: Matlab simulation of three dimensional granule interactions in a granulator.

ity, moisture content, liquid fraction, and pore saturation for each particle are also determined.

A forward discrete approximation of Equation 27 is used to model consolidation in each granule at each time step. Consolidation clearly only affects the volume of air present in each granule. This escape of air changes the porosity, moisture fraction, pore saturation and liquid fraction of each granule. As compaction continues and granule G_i approaches a critical pore saturation, S^*, Equation 5 is used to calculate the formation and growth of the viscous binder layer. The critical pore saturation used in this simulation was $S^* = 0.85$.

Once the binder layer thickness is calculated, the asperity height is estimated. Asperity height is a parameter that stays relatively constant over a simulation because the size of the constituent particles will remain the same. The height of the surface asperities is assumed to be proportional to the size of the constituent particles making up the the granule:

$$h_a = AD_p \tag{34}$$

where A is a proportionality constant less than or equal to 0.5. ($A = 0.5$ for these simulations) and D_p is the diameter of the particles making up the granule. This proportionality constant is dependent on the process. To simplify this parameter, the constituent particles were assumed to be on the order of a micron and $A = 0.1$, creating a constant asperity height of $h_a \cong 1 \times 10^{-7} m$. With this value for the height surface asperities, the ratio of the binder layer thickness to asperity height is found to commonly be $h_0/h_a \cong 0.1$, a value commonly used in literature [31, 8].

The granule yield strength is then calculated for each time step using the following assumptions: the shape factor $C = 6$, the solid-liquid contact angle is zero, and a the binder surface tension and solid Poisson ratio are known. The yield strength is calculated using Equation 17. The deformation of the particle is also calculated at each time step using Equation 22, where the granule initial velocity is:

$$u_0 = \sqrt{v_{x_i}^2 + v_{y_i}^2 + v_{z_i}^2} \tag{35}$$

The deformation of the particle at each time step will be critical, because when the granule deformation exceeds the critical value $St_{def}^* = 0.1$, then the particle is assumed to be in a shear field capable of tearing the particle into two constituent particles each assumed to be one-half the volume of the original:

$$\begin{aligned}(s_i\,, l_i\,, a_i) &= \left(s_{i/2}\,, l_{i/2}\,, a_{i/2}\right) + \left(s_{i/2}\,, l_{i/2}\,, a_{i/2}\right) \\ &= (s_j\,, l_j\,, a_j) + (s_k\,, l_k\,, a_k)\end{aligned} \tag{36}$$

Each granule is now described by a vector of several known quantities:

$$\begin{aligned}G_i = [&v_x \quad v_y \quad v_z \quad x \quad y \quad z \quad V \quad D \\ &s \quad l \quad a \quad \varepsilon \quad L \quad S \quad h_0 \quad h_a \quad Y_d \quad St_{def}]^T\end{aligned} \tag{37}$$

With each of parameter of the granule known in the vector G_i, the simulation progresses incrementally each representative time step for the particles within the control volume. Periodic boundary conditions are assumed at the walls of the control volume. The density of particles in the simulated control volume is higher than normal to increase the representative rate of particle interaction. If this compression is not performed, small steps in time will be required, resulting in relatively few particle-particle interactions per iteration and long simulation times. Due to the compression of control volume, the particle velocities must also be decreased by a factor of 10^4 so that particle interactions are not overlooked. This dilation factor can be established such that each particle moves a length approximately equal to the diameter of a particle at each simulation step. The actual velocities of the individual particles are used for determination of the results of interaction and breakage.

Particles move at a rate based on their velocity until the radius of one particle encounters another particle. If there is a binder layer present, either Type I or Type II coalescence is possible. For particles with a binder layer present u_1 is calculated from Equation 7. The mean harmonic mass and diameter of the two colliding particles is calculated, thereby allowing the viscous Stokes number for the two particles to be calculated. Type I coalescence is determined based on the criteria set in Equation 11 where h_0 and h_a are the mean binder layer thickness and mean asperity height of the colliding particles. If the conditions are such that coalescence occurs, the volumes of solid, liquid, and gas are added to form the new particle. The

two constituent granules are destroyed and a new one is created with volumes shown in Equation 38.

$$\begin{aligned}(s_i\,,l_i\,,a_i)+(s_j\,,l_j\,,a_j) &= (s_i+s_j\,,l_i+l_j\,,a_i+a_j)\\ &= (s_k\,,l_k\,,a_k) \end{aligned} \quad (38)$$

If Type I coalescence does not occur, rebound velocities u_2 and u_3 are calculated from interactions created by the collision. If the final rebound velocity, u_3 is greater than zero, then no coalescence occurs and the particles "bounce" off each other. These rebounding particles are then given velocities equal to their collision velocities, but in the opposite direction. This assumes each collision has a coefficient of restitution of one, regardless of the actual coefficient of restitution for the particle. Coalescence of surface wet particles is based on the criteria set in Equation 21. If Type II coalescence does occur, a new granule is created in the same manner as for Type I coalescence. For granules without a binder layer present, as in the induction period, coalescence or rebound is determined based on the criteria set in Equation 25. For each new particle "born", a new vector G_j will be created with parameters calculated using new solid, liquid, and air volumes from Equation 38.

One may assume that granules will continue to coalesce until they reach a critical granule size above which granulation becomes impossible. This critical size is represented in PBE models as the size independent kernel, β_0. This constant kernel is commonly used to represent a higher probability of coalescence between particles at lower size classes. Ouchiyama and Tanaka [35] derived a critical granule size for deformable particles. They assumed that highly deformable particles had a larger contact area, thereby decreasing the chance of particle breakup and increasing growth rate. From the torque forces and binding forces acting on a deformed granule at the contact area, Ouchiyama and Tanaka derived the following equation:

$$D^* = A_1\left(K^{3/2}\sigma_t\right)^{a_1} \quad (39)$$

where A_1 and a_1 are constants independent of granule size for a system, σ_t is the granule tensile strength given in Equation 16, and K is a measure of the granule deformability, a ratio of the contact area between granules and the force of the granule impact. The force of colliding granules in the approach stage was derived in Liu [31],

$$F = \frac{3}{4}\pi\widetilde{D}^2\mu\frac{u}{2h} \quad (40)$$

where $2h$ is the distance between approaching granules, commonly assumed to be the binder layer thicknesses. The contact area is related to the permanent deformation, δ'', by:

$$A = \pi\widetilde{D}\delta'' \quad (41)$$

Table 1: Initial distribution for simulation.

$i\,(-)$	$v_i\ (m^3)$	$d_i\ (\mu m)$	$N_{itot}\,(-)$	$q_i\ (m^3)$
1	2.00×10^{-12}	156	120	2.40×10^{-10}
2	4.00×10^{-12}	197	42	1.68×10^{-10}
3	6.00×10^{-12}	225	20	1.20×10^{-10}
4	8.00×10^{-12}	248	5	4.00×10^{-11}
5	10.0×10^{-12}	267	5	5.00×10^{-11}

In this simulation, the constant A_1 was taken to be a function of granule moisture content to allow granules with higher liquid content to also have a larger critical granule size to follow experimental results found by several groups ([39, 45, 47]). For the simulation $a = 1/2$ and $A_1 = 0.002w^{1/4}$. Once coalescence criteria are determined, the new granule diameter is calculated and compared to the critical granule size, D^*. If $D > D^*$, then coalescence does not occur and the particles rebound as normal.

4 Results and discussion

4.1 Discrete element simulation parameters

Several initial particle size distributions were simulated. In order to compare results from this simulation to results found using analytical solutions of PBE models, the initial size distribution and volume fractions used by Pouw et al. [37] were used for validation. The particles were separated into five size classes by particle volume, v_1, v_2, v_3, v_4, and v_5. The initial solid volume fraction of each granule was 0.52, the liquid volume fraction was 0.33, and the air volume fraction was 0.15. The proposed dynamic simulation will only examine a small fraction of the granules that would be present in a real process, but trends will be evident even with the small sampling size. The simulations can be run multiple times to develop an ensemble average PSD. The simulation used by Pouw et al. measured the change in granule quantities, q_s , q_l, and q_a at each size class. The quantities are the total volume of solids, liquid, or air of granules at each size class. Table 1 shows the initial distribution of particles used in the first simulation. Initially, 192 particles were used. Particles separated into each of the five size classes were given the same initial volumes. These particles were examined in a $8\times10^{-9}\,m^3$control volume.

4.2 Simulation results

The discrete element simulation ran 50 times and the results were averaged. Figure 5 shows the results found using discrete element simulation approach with the initial

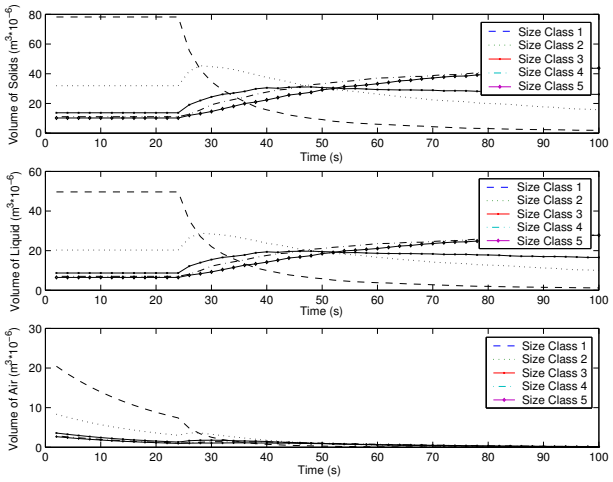

Figure 5: The change of volume in the solid, liquid and air (top to bottom) for each of the five volume classes simulated. The size classes begin in ascending order, smallest granules to largest.

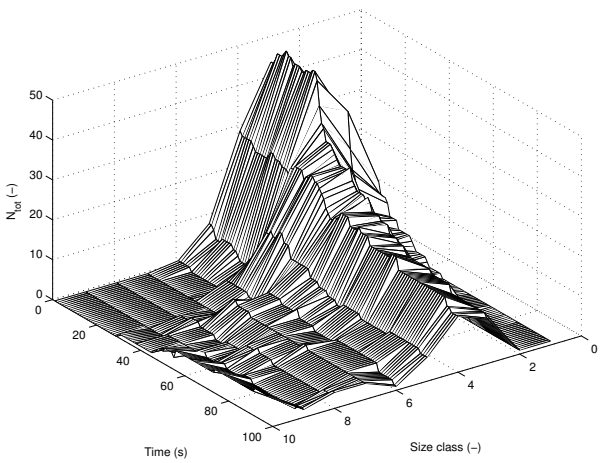

Figure 6: Evolution of PSD for particles with new initial conditions.

distribution given by Pouw et al. [37] The analytical solution of the PBE derived by Pouw et al. [37] produced results that were very similar to Figure 5. Pouw et al. [37] used a coalescence kernel primarily based on pore saturation of the granule reaching a critical value. This kernel takes into account Type I coalescence and neglects Type II coalescence. Furthermore, breakage was not taken into account in the model proposed by Pouw et al. The size independent coalescence kernel, β_0, used by Pouw et al. was chosen in order to allow smaller particles a greater chance of coalescence.

This same phenomenon was taken into account with the dynamic simulation by determining the proper parameters for the critical granule size at which point coalescence becomes impossible, D^*. For this simulation, the constants based on the process, A_1 and a, were 0.00156 and 1/2 respectively. From these results, an induction period followed by rapid growth is evident. Granules begin the simulation with a dry surface. Consolidation continues throughout the simulation until the pores reach the critical saturation and binder is forced to the surface. This occurs at the simulation after roughly 20 time steps. The surface dry granules are not deformable to coalesce due to Type II coalescence. Therefore, all coalescence occurs following the formation of the viscous binder layer. Despite looking at a small sample size, the results of the dynamic simulation still show the trends of an analytical solution that could be modeling nearly an infinite number of particles.

The process of consolidation is evident in Figure 5 for the change in the quantity of air, Q_a over the simulation period. Since consolidation affects only air, the quantities of solid and liquid in the granules are unaffected. Figure 5 shows a good representation of how a granule is compressed until the binder layer is present and rapid growth occurs. Since the minor effect of evaporation was neglected, the quantity of the solids and the liquid in the granule at each of the five size classes were identical.

This simulation process is flexible enough to examine a variety of process conditions. Several other simulations were run with substantially different initial conditions. To track the evolution of a PSD at typical conditions, a simulation was run that used an initial normal distribution of particles with a mean volume of $3\times10^{-12}\,m^3$ with a standard deviation of $1\times10^{-12}\,m^3$. The particles were classified by size into 10 size classes for graphical presentation purposed. Class 1 consisted of particles whose volumes ranged between 0 and $1\times10^{-12}\,m^3$, the second class consisted of particles whose volumes ranged between 1 and $2\times10^{-12}\,m^3$ all the way up to the tenth class which consisted of particles whose volumes were greater than $9\times10^{-12}\,m^3$. The velocity distribution and granule composition was the same as the previous test. The simulation was run for 100 representative time steps. The evolution of the PSD is shown in Figure 6 for a single simulation. The volume change for each of the 10 size classes was averaged over 50 simulations to produce the results shown in Figure 7.

A simulation was run to demonstrate the effect of impeller speed on the evolution of the PSD. There is an important trade-off to the effect that impeller speed has on either increasing the mean particle size or decreasing it. Knight et al. [26] describe how the effect of impeller speed is very complex, showing experimental results where increased impeller speed increases the rate of coalescence between particles due to the increased interactions until breakage occurs. Granule interactions at low impeller speed usually result in Type I coalescence or re-

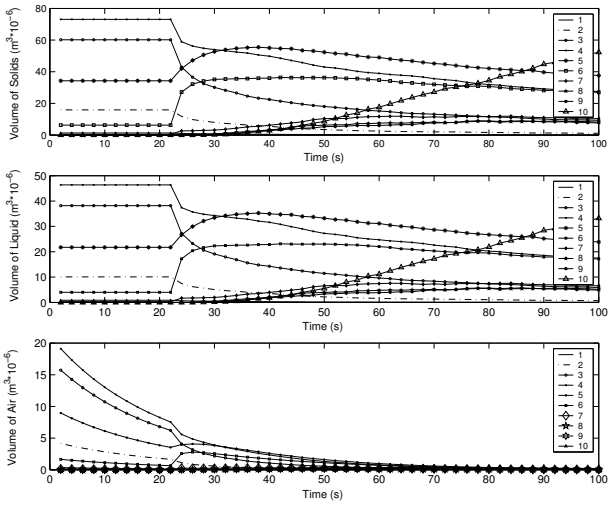

Figure 7: Volume change for solid, liquid, and air (top to bottom) for all 10 size classes in simulation 2.

Table 2: Result of granular interactions at three impeller conditions.

Interaction	120 rpm	360 rpm	720 rpm	840 rpm
Type I coal.	6.1%	5.9%	5.0%	4.5%
Type II coal.	3.2%	7.5%	8.4%	11.0%
Rebound	90.7%	86.6%	86.6%	84.5%
Means size (μm)	219.6	233.5	237.5	229.3

bound due to the fact that the impact velocity may not be great enough to break the binder layer or to create deformation. These interactions result in weakly bonded granules because Type I coalesced granules are not as strong as granules produced from deformed granules. Despite the weakness of these bonds, rapid growth can still occur at low impeller speeds due to the lack of a shearing force, especially when excess binder is present. At high impeller speeds, more interactions between particles occur. If the conditions are suitable for coalescence, rapid growth may result. However, high impeller speeds often result in collisions involving kinetic energy far greater than what can be dissipated by the binder layer. This results in far more rebound events than collisions at lower speeds. Simulations were run at four impeller speeds: mean granule velocities of $v_i = 7\ m/s$ with a standard deviation of 1 m/s, $v_i = 6\ m/s$ with a standard deviation of 1 m/s, $v_i = 3\ m/s$ with a standard deviation of 1 m/s, and $v_i = 1\ m/s$ with a standard deviation of 1 m/s. These mean granule velocities correspond to 840, 720, 360 and 120 rpm respectively using Equation 33 and assuming a granulator diameter of 1 m. The result of their interactions are listed in Table 2.

Table 2 shows that low impeller speed produce predominantly Type I coalesced granules, while higher impeller speeds mainly produce Type II coalesced granules. This intuitively makes sense due to the increased deformation associated with tests at higher impeller speeds. Studies to determine the effects of impeller speed on granule size and size distribution have produced conflicting results [42, 36]. Schaefer et al. [42] reports that the increases in the Stokes number due to greater impeller speed increase the rate of growth since the system becomes more deformable. This growth continues until disruptive shear forces balance the growth forces in the process. To an extent, this fact is evident in the result depicted in Figure 8. Rapid growth is shown in all instances except during the initial stages of the highest impeller speed tested. At this speed, the shear forces were great enough to break several particles resulting in a smaller PSD. However, in the experimental results from Sheafer et al. [42], all impeller speeds undergo a similar disruptive breakage process except the lowest impeller speed, resulting larger particles corresponding to the lowest impeller speed, 200 rpm. Oulahna et al. [36] present data which corresponds with the data presented here. Oulahna et al. report that initially there are fewer fines associated with higher impeller speed. This is evident in Figure 8, as seen by the smaller particles associated with the lower impeller speeds. These fines can be attributed by the larger number of unsuccessful collisions (largely Type II collisions) in the lowest impeller speed test shown in Table 2. Oulahna et al. also report that as the impeller speed increases, the size distribution gets narrower. This is evident as well in Figure 8. They also suggest that there are more fines at the higher impeller speed than the middle speeds (720 rpm, 360 rpm) due to the fact that there is more breakage at higher shear forces. the breakage of particles was determined by calculating the critical Stokes Deformation number for each particle to see if it was greater that a critical value ($St^*_{def} = 0.2$).

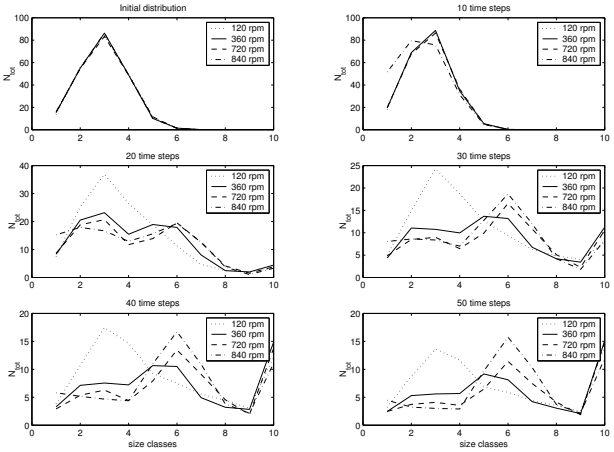

Figure 8: PSD evolution for simulations run at 120 rpm, 360 rpm, 720 and 840 rpm.

Open-loop simulations were also performed to examine the effect binder content had on coalescence of granules.

Table 3: Result of granular interactions at three binder conditions

Interaction	15% binder	25% binder	33% binder	40%
Type I coal.	1.6%	3.9%	5.9%	6.
Type II coal.	3.4%	5.4%	7.5%	8.
Rebound	95.0%	90.7%	86.6%	85.
Mean size (μm)	199.9	222.9	233.5	23

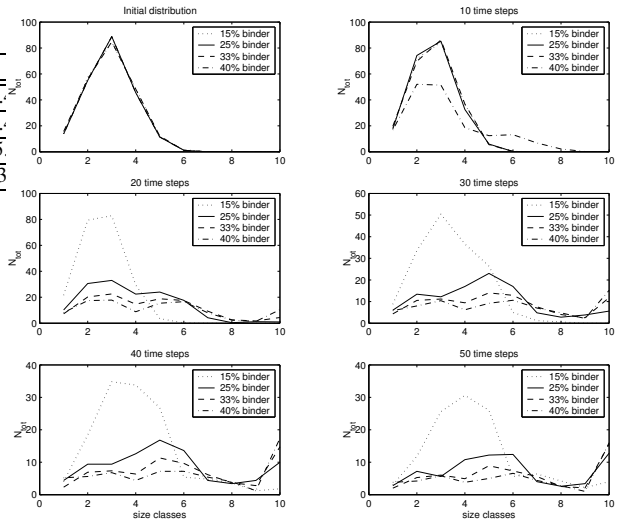

Figure 9: PSD evolution for simulations run at 15%, 25%, 33%, and 40% binder content.

Three initial conditions were examined, all with medium values of impeller speeds. Condition 1 had a solid volume fraction of 0.7, a liquid volume fraction of 0.15, and an air volume fraction of 0.15. Condition 2 had a solid volume fraction of 0.6, a liquid volume fraction of 0.25, and an air volume fraction of 0.15. Condition 3 had a solid volume fraction of 0.52, a liquid volume fraction of 0.33, and an air volume fraction of 0.15. Finally, condition 4 had a solid volume fraction of 0.45, a liquid volume fraction of 0.40, and an air volume fraction of 0.15. Thirty simulations were performed over 100 time steps and again were averaged. The results of particle interactions are listed in Table 3. This table clearly shows that as the moisture content increases, the mean particle size also increases. The dependence of granule size on liquid saturation has been studied with similar results from several groups ([10, 39, 9]). Table 3 also presents several other interesting facts. As the liquid content in the granules increased, the number of successful granule collisions clearly increased as well. This was most evident with the Type II coalescence. As liquid is added to granules, they become more deformable, thus allowing more successful Type II collisions to take place. Another reason for the reduced number of successful collisions is the fact that granules with a lower liquid content require more consolidation to reach the capillary state of saturation in which rapid granule growth is possible. In the lowest binder level, 15% liquid, the induction period is far longer than in simulations with more binder initially present in the granule. This is clearly due to the fact that it will take a longer period of consolidation for granules to reach a critical pore saturation. Hence, increasing binder content decreases induction time. This mirrors findings by Hoornaert et al. [13]. A comparison of the evolution of the PSD's for each of these four binder conditions is displayed in Figure 9. With the addition of more binder, these granules would enter a slurry regime due to a maximum pore saturation greater than one as described by Iveson et al. [15]. Oversaturated granules tend not to coalesce well despite their high deformability. Once oversaturated, granules reach a state described by Iveson and Litster [15] as a slurry or overwet mass. There are other factors that come into account when pores are over saturated. Granules may break shortly after forming because the yield strength of large deformable particles is not great. Furthermore, above the critical granules size at which coalescence becomes impossible, wet powder masses are too weak to form granules, thereby producing smaller granules at high binder levels. Particle growth is more difficult to predict than simply stating that it is primarily a factor of pore saturation or liquid content. Other properties such as granule yield strength, tensile strength, and the shear force in the granulator will affect the final PSD.

Granule growth regime maps are common methods of showing growth rates of a granulation process by simply determining the viscous Stokes number and Stokes deformation number for a group of particles. Coalescence boundary maps are also popular methods of presenting theoretical results showing what conditions are beneficial to result in Type I, Type II, or rebound during a simulation [15, 20]. Coalescence boundary maps are dependent on several sets of important dimensionless parameters:

- St_v , the viscous Stokes number, the ratio of the kinetic energy caused by granule collisions with respect to the viscous dissipation of the binder layer.
- St_{def}, the Stokes deformation number, the ratio of the kinetic energy caused by granule collisions with respect to the plastic deformation of the granule.
- h_0/h_a, the ratio of the liquid binder layer to the height of the surface asperities. This determines the ability for granules to undergo surface wet coalescence.
- h_0/δ, the ratio of the liquid binder thickness to the permanent granule deformation. This parameter is dependent on St_{def} and St_v .
- $\widetilde{D}/h_0$, the ratio of the mean harmonic granule diameter to the thickness of the liquid binder layer.

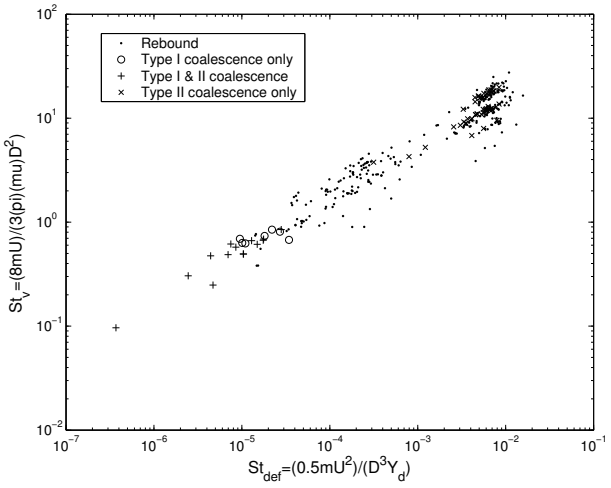

Figure 10: Results of granule interactions for a sample simulation.

– Y_d/E^*, the ratio of the granule plastic yield stress to the elastic modulus.

Typical coalescence boundary maps consider these dimensionless parameters to be constant, but clearly during induction and rapid growth stages of a granulation process or a simulation, these parameters will be dependent on other factors. The results of granule interactions for one simulation with the initial conditions given in Table 1 are shown in Figure 10. Clearly, hard coalescence boundaries are not available when looking at a simulation of a process in which the pore saturation of the granules increases. This simulation lasted for 100 time steps and included 320 granule-granule interactions. Of these interactions 82% resulted in rebound, 4% resulted in conditions that fit criteria for both Type I and Type II coalescence,12% resulted in Type II coalescence only, and 2% resulted in Type I coalescence only. Of the the 4% that could be either Type I or Type II, these are assumed to be Type I since it would occur prior to Type II coalescence. Since the boundaries of coalescence change with the degree of pore saturation or porosity of granules, it would be pointless to overlay a coalescence boundary map on Figure 10. Despite this, there are still some inferences that can be made. Type I coalescence criteria, Equation 11, is independent of the value of the Stokes deformation number, so the boundary for Type I coalescence will always be a horizontal line towards the minimum values of the viscous Stokes number. As pore saturation increases, this boundary for Type I coalescence increases. Figure 10 does show Type I coalescence occurring in areas of low viscous Stokes numbers.

Clearly, as Figure 10 shows, there are no clear boundaries present. There are areas where Type I coalescence is more likely to occur, however, situations which result in low viscous Stokes numbers. Also, Figure 10 shows that the boundary for rebound and Type II coalescence moves as the porosity of the granules increases. Type II coalescence occurred at interactions that resulted in viscous Stokes numbers an order of magnitude greater and Stokes deformation numbers almost two orders of magnitude greater than interactions resulting in Type I coalescence. Rather than create coalescence boundary maps based on constant values of dimensionless parameters that are regardless of the current values of the granules, these values could be described relative to the porosity or pore saturation that the granules are currently experiencing. Liu et al. [31] generated coalescence boundary maps where the following constant values were used: $Y_d/E^* = 0.01$, $h_0/h_a = 10$, and $D/h_0 = 100$. For a given simulation with initial conditions listed in Section 4.1, the porosity will decrease from 0.47 to the minimum porosity of 0.389. Due to consolidation, the dimensionless parameters are not necessarily constant; they will change depending on the current granular conditions.

5 Conclusions

The use a dynamic discrete element simulation of particle interactions has proven to be an effective method of modeling and simulating particle-enlargement techniques such as granulation. The proposed method uses knowledge of individual particle properties rather than group quantities of particles into classes as in the case of population balance methods. Despite the differences between this method and current modeling techniques using population balance equations, this method was shown to produce very similar results to PBE methods given certain assumptions. This dynamic simulation method also allows for broad changes to granule properties to account for changes in granule composition and changes in physical interactions. This method allows for an improved examination of granule interactions. One can determine whether a process is more likely to undergo Type I coalescence or Type II coalescence. One may examine what process conditions are unfit for coalescence to occur. Rate processes such as consolidation can be included to the simulation to create a dynamic induction effect where rapid growth follows when a binder layer appears. Other less important rate processes, such as attrition and layering, could also be included in future work. Breakage was included in the simulation by determining breakage criteria based on a critical strain rate or a critical Stokes deformation number. Breakage does not come into effect unless the impeller speed is great enough to create a shearing force to break the particles. In the simulations presented in this work, the impeller was at a constant angular velocity of 3 m/s.

Open loop simulations were performed that compared PSD's over time for processes with differing binder content and impeller speeds. High impeller speed were shown to create a strong shear field in which large granules were broken. At higher impeller speeds, however, a narrower PSD was present. While the lower impeller speeds did not result in as many successful Type II collisions, the low collision velocity resulted in a very high amount of Type I collisions. These Type I collisions produce large particles held together by weak viscous forces. Type II collisions produce stronger aggregate particles. Higher impeller speeds produce additional Type II collisions, and the resulting granules may be more beneficial as a final product.

A comparison of initial binder contents was also simulated. The simulation in which the lowest binder content was used resulted in the least number of successful collisions and the smallest mean granule size. As the binder content in each granule increased, the number of successful Type I and Type II collisions increased as well,. Therefore, larger granules are present in simulations with more binder present. This is in agreement with conclusions found by several other reported results [9, 10, 39].

Acknowledgements

The authors gratefully acknowledge the helpful comments of the anonymous reviewers and financial support from the University of South Carolina Center for Manufacturing and Technology.

6 Nomenclature

a_i Air volume of granule i
A Asperity height proportionality constant
A^* Maximum deformation area
A_1 Size independent parameter for critical granule size
a_1 Size independent parameter for critical granule size
$\beta(u, v)$ Coalescence kernel
β_0 Size independent coalescence kernel
$\beta^*(u, v)$ Size dependent coalescence kernel
C Shape factor
δ^* Maximum compression distance
δ' Extent of elastic recovery
δ'' Maximum deformation
D Granule diameter
D_g Granulator diameter
D_p Basic particle diameter
D^* Critical granule diameter
$\widetilde{D}$ Mean harmonic diameter
ϵ_i Porosity of granule i
ϵ_{min} Minimum attainable granule porosity
ϵ_m Granule strain
ϵ_m^* Critical granule strain
E^* Effective Young's modulus
E_i Young's modulus of granule i
F Force of colliding granules
γ Strain rate in Hershel-Buckley model
γ_l Liquid surface tension
$2h$ Distance between approaching granules
h_a Surface asperity height
h_o Liquid layer thickness
K Measure of granule deformability
k_c Consolidation rate constant
l_i Liquid volume of granule i
L_i Liquid fraction of granule i
m_i Mass of granule i
$\widetilde{m}$ Mean harmonic mass
n Flow index in Hershel-Buckley model
μ Binder viscosity
ω Angular velocity of impeller
P Mean contact pressure
P_o Maximum contact pressure
ρ_a Density of air
ρ_l Density of liquid
ρ_s Density of solid
σ_t Maximum tensile stress
S_i Pore saturation of granule i
s_i Solid volume of granule i
St_v Stokes number
St_{def} Stokes deformation number
St_{def}^* Critical stokes deformation number
θ Solid-liquid contact angle
τ Yield stress of Hershel-Buckley model
u_o Initial relative velocity of colliding particles
u_1 Approach velocity of colliding particles
u_2 Deformation velocity in Type II collision
v_i Poisson ratio
w_i Moisture fraction of granule i
V_i Total volume of granule i
v_{x_i} Velocity of granule i in x direction
Y_d Plastic yield stress

References

[1] A. A. Adetayo and B. J. Ennis. A unifying approach to modeling coalescence mechanisms. *AIChE*, 43(1):927–934, 1997.

[2] A. A. Adetayo and B. J. Ennis. A new approach to modeling granulation processes for simulation and control purposes. *Powder Technology*, 108:202–209, 2000.

[3] A. A. Adetayo, J. D. Litster, S. E. Pratsinis, and B. J. Ennis. Population balance modeling of drum granulation of materials with wide size distribution. *Powder technology*, 82:37–49, 1995.

[4] A. Annapragada and J. Neilly. On the modeling of granulation processes: a short note. *Powder Technology*, 89:83–84, 1996.

[5] R. J. Batterham, J. S. Hall, and G. Barton. Pelletizing kinetics and simulation of full scale balling circuits. *Proceedings of the 3rd International Symposium on Agglomeration*, Nurnberg, W. Germany:A136, 1981.

[6] Steve Bull. Elastic contact stress formulae. www.staff.ncl.ac.uk/s.j.bull/ecsttr.html, 1999.

[7] S. A. Cryer. Modeling agglomeration processes in fluid-bed granulation. *AIChE*, 45(10):2069–2078, 1999.

[8] B. J. Ennis. A microlevel-based characterization of granulation phenomena. *Powder Technology*, 65:257–272, 1991.

[9] B. J. Ennis. Agglomeration and size enlargement session summary paper. *Powder Technology*, 88:203–225, 1996.

[10] B. J. Ennis and J. D. Litster. *Perry's Chemical Engineers' Handbook*, chapter Particle size enlargement, pages 20–56–20–89. McGraw Hill, 7th edition, 1997.

[11] K. Heiskanen. On the difficulties of implementing particle size control in particulate processes. *Powder Technology*, 82:13–19, 1995.

[12] B. Hess and R. M. Scheek. Orientation restraints in molecular dynamics simulation using time and ensemble averaging. *Journal of Magnetic Resonance*, 164:19–27, 2003.

[13] F. Hoornaert, P. Wauters, G. Meesters, S. Pratsinis, and B. Scarlett. Agglomeration behavior of powders in a lodige mixer granulator. *Powder technology*, 97:116–128, 1998.

[14] M. J. Hounslow, R. L. Ryall, and V. R. Marshall. A discetized population balance for nucleation, growth and aggregation. *AIChE Journal*, 34(11):1821–1832, 1988.

[15] S. Iveson and J. Litster. Growth regime map for liquid-bound granules. *AIChE Journal*, 44:1510–1518, 1998.

[16] S. Iveson, J. Litster, and B. Ennis. Fundamental studies of granule consolidation. part 1: effects of binder content and binder viscosity. *Powder Technology*, 88:15–20, 1996.

[17] S. M. Iveson. Limitations of one-dimensional population balance models of wet granulation processes. *Powder Technology*, 124:219–229, 2002.

[18] S. M. Iveson, J A. Beathe, and N. W. Page. The dynamic strength of partially saturated powder compacts: the effect of liquid properties. *Powder Technology*, 127:149–161, 2002.

[19] S. M. Iveson, J. D. Litster, K. Hapgood, and B. J Ennis. Nucleation, growth and breakage phenonmena in agitated wet granulation process: a review. *Powder technology*, 117:3–39, 2001.

[20] S. M. Iveson, P. A. L. Wauters, S. Forrest, J. D. Litster, G. M. H. Meesters, and B. Scarlett. Growth regime map for liquid-bound granules: further development and experimantal validation. *Powder Technology*, 117:83–97, 2001.

[21] K. L. Johnson. *Contact Mechanics*. Cambridge University Press, 1987.

[22] P. C. Kapur. Kinetics of granulation by non-random coalescence mechanism. *Cemical Engineering Science*, 27:1863–1869, 1972.

[23] P. C. Kapur and D. W. Fuerstenau. *Trans. AIME*, 229:348–355, 1963.

[24] P. C. Kapur and D. W. Fuerstenau. Coalescence model for granulation. *Industrial and Engineering Chemistry, Process Design Devices*, 8:56–62, 1969.

[25] S. Kenningley, P. Knight, and A. Amrson. An investigation into the effect of binder viscosity on agglomeration. *Powdeer Technology*, 91:95–103, 1997.

[26] P. Knight, A. Johansen, H. Kristensen, T Schaefer, and J. Seville. An investigation of the effects on agglomeration of changing the speed of the mechanical mixer. *Powder Technology*, 110:204–209, 2000.

[27] H. G. Kristensen, P. Holm, and T. Schaefer. Mechanical propeties of moist agglomerates in relation to moist agglomerates. *Powder Technology*, 44(227-247), 1985.

[28] S. Kumar and D. Ramkrishna. On the solution of population balance equations by discretization-i. a fixed pivot technique. *Chemical Engineering Science*, 51:1311–1332, 1996.

[29] S. Kumar and D. Ramkrishna. On the solution of population balance equations by discretization-ii. a moving pivot technique. *Chemical Engineering Science*, 51:1333–1342, 1996.

[30] T. Lee and R. S. Lake. Anisotropic polyurethane foam with Poisson's ratio greater than 1. *Journal of Membrane Science*, 32:2397–2401, 1997.

[31] L. X. Liu and J. D. Litster. Coalescence of deformable granules in wet granulation processes. *AIChE Journal*, 46(3):529–539, March 2000.

[32] L. X. Liu and J. D. Litster. Population balance modeling of granulation with a physically based coalescence kernel. *Chemical Engineering Science*, 57:2183–2191, 2002.

[33] H. Marques and K. Brown. Molecular mechanics and molecular dynamics simulations of porphyrins, metalloporphyrins, heme protiens and cobalt corrinoids. *Coordination Chemistry Reviews*, 225:123–158, 2002.

[34] M. Matsumoto. Molecular dynamics of fluid phase change. *Fluid phase equilibria*, 144:307–314, 1998.

[35] N. Ouchiyama and T. Tanaka. *I and EC Process Design and Dev.*, 21(29-35), 1982.

[36] D. Oulahna, F. Cordier, L. Galet, and J. A. Dodds. Wet granulation: the effect of shear on granule properties. *Powder Technology*, 130:238–246, 2003.

[37] G. A. Pouw, D. Verkoeijen, G. M. H. Meesters, and B. Scarlett. Population balances for particulate processes-avolume approach. *Chemical Engineering Science*, 57:2287–2303, 2002.

[38] D. Ramkrishna. The status of population balances. *Rev. Chem. Engng*, 3:49–95, 1985.

[39] M. Ritala, P. Holm, T. Schaefer, and H. Kristensen. Influence of liquid bonding strength on power consumption duirng granulation in a high shear mixer. *Drug Dev. Ind. Pharm.*, 14:1041–1060, 1988.

[40] H. Rumpf. The strength of granule and agglomerates. *AIME, Agglomeration, Interscience*, pages 379–418, 1962.

[41] K. V. S. Sastry. Similarity size distribution of agglomerates during their growth by coalescence in granulation or green pelletization. *International Journal of Mineral Processing*, 2:187–203, 1975.

[42] T. Schaefer, P. Holm, and H. G. Kristensen. Wet granulation in a laboratory scale high shear mixer. *Pharm Ind.*, 52:1147–1153, 1990.

[43] M. Song, A. Steiff, , and P. M. Weinspach. A very effective new method to solve the population balance equation with particle size growth. *Chemical Engineering Science*, 52(20):3493–3498, 1997.

[44] I. Talu, G. Tardos, and M. I. Khan. Computer simulation of wet granulation. *Powder Technology*, 110:59–75, 2000.

[45] G. Tardos, M. I. Khan, and P. R. Mort. Critical parameters limiting conditions in binder granulation of fine powders. *Powder Technology*, 94:245–258, 1997.

[46] P. Wauters. *Modeling and mechanisms of granulation*. PhD thesis, Delft University of Technology, Delft, The Netherlands, 2001.

[47] P. A. L. Wauters, R. B. Jacobsen, J. D. Litster, G. M. H. Meesters, and B. Scarlett. Liquid distribution as a means to describe the granule growth mechanism. *Powder Technology*, 123:166–177, 2002.